Original scientific paper

CONVECTIVE FLOW AND HEAT TRANSFER OF NANO-ENCAPSULATED PHASE CHANGE MATERIAL (NEPCM) DISPERSIONS ALONG A VERTICAL SURFACE

Mohammad Ghalambaz[1,2], Haichuan Jin[3], Amirhossein Bagheri[4], Obai Younis [5,6], Dongsheng Wen[3,7]

[1]Metamaterials for Mechanical, Biomechanical and Multiphysical Applications Research Group, Ton Duc Thang University, Ho Chi Minh City, Vietnam
[2]Faculty of Applied Sciences, Ton Duc Thang University, Ho Chi Minh City, Vietnam
[3]School of Aeronautic Science and Engineering, Beihang University, Beijing, P.R. China
[4]Department of Mechanical Engineering, Shiraz University, Shiraz, Iran
[5]Department of Mechanical Engineering, College of Engineering in Wadi Addwasir, Prince Sattam Bin Abdulaziz University, KSA
[6]Department of Mechanical Engineering, Faculty of Engineering, University of Khartoum, Sudan
[7]Lehrstuhl für Thermodynamik, Technische Universität München, Garching, Germany

Abstract. *Nano-encapsulated phase change suspension is a novel type of functional fluid in which the nanoparticles undergo phase change that contribute to heat transfer. Thus, the working fluid carries heat not only by sensible heat but also in the form of latent heat stored in the particles. The natural convection and heat transfer of Nano-Encapsulated Phase Change Materials (NEPCMs) suspensions within a boundary layer along a heated flat surface are theoretically investigated in this work. The nanoparticles are core-shell structured with the core fabricated from PCMs covered by a solid shell. A similarity solution approach along with the finite element method is employed to address the phenomena. The outcomes indicate that a decisive factor in boosting the heat transfer is the temperature at which NEPCM particles undergo the phase transition. The heat transfer parameter can be enhanced by about 25% by just adding 5% of NEPCM particles, compared to the case with no NEPCM particles.*

Key words: *Nano-encapsulated phase change materials; Phase change materials; Boundary layer heat transfer enhancement; similarity solution.*

1. INTRODUCTION

Heat transfer is one of the important major demands of recent technological advancement in electronic packaging, aerospace and avionics systems, power engineering, and high-power x-ray devices. These devices produce a tremendous amount of waste heat in confined space, requiring efficient cooling systems to extract the produced heat, and transfer it to the surrounding. The most challenging aspect of thermal control of surfaces with high heat-flux-density is heat removal from the surface. Moreover, many of high-power devices are sensitive not only to the high temperatures but also to the temperature gradients across the surface of the device. The temperature gradient within a device would produce mechanical stress that may damage the sensitive structures of the device. Therefore, new working fluids or new techniques capable of enhancing heat transfer or inducing a uniform temperature distribution are of high interest. In this regard, phase change materials, nanofluids, and NEPCMs are introduced as promising passive ways to facilitate heat transfer and improve thermal management.

A phase change material (PCM) benefits from a large latent heat thermal storage at a fusion temperature. This remarkable quality has drawn researchers' attention towards potential applications of PCMs in heat storage and heat sink technologies. Construction [1, 2], homes and offices air conditioning systems [3], space heating/cooling, and waste heat recovery in different industries are just a few areas that using PCM can exceptionally be beneficial.

About two decades ago, nanofluid was introduced as a stable suspension of nanoparticles into a base fluid to enhance heat transfer [4]. Although nanoparticles can notably boost the heat transfer of a base fluid, they also have the drawback of reducing the working fluid's heat capacity, which is not good for many applications [5]. When the heat capacity of fluid is low, the temperature gradient along the cooling fluid increases. The Nano-Encapsulated PCM (NEPCM) are nanoparticles comprising a core and a shell. A phase change material such as paraffin, n-tetradecane, or octadecane is used in manufacturing the core, and the shell is usually made of a polymer [6, 7]. A stable suspension of NEPCM nanofluid can effectively remove a large amount of heat from a hot surface using the latent heat of NEPCM particles. The other important advantage of NEPCMs is the temperature control of a coolant at the fusion temperature. Indeed, NEPCMs tend to remain at their fusion temperature and go through a phase change.

Due to important applications of PCMs and recent advancement in the improvement of these materials using nanotechnology, Sarkar et al. [8] and Sidik et al. [9] explored the thermal advantages of using nanofluids and phase change materials for energy storage applications. Sidik et al. [9] addressed the key factors that affect the enhancement of heat transfer of PCMs, including the shape and size of NEPCMs, and shell fraction of nanoparticles. Sarkar et al. [8] concluded employing encapsulated PCM in building components for cold storage applications could improve the energy saving. Shah [10] reviewed the nanotechnology aspect of PCMs by focusing on the synthesis technique and materials/morphology of PCMs and their influence on thermal-conductivity enhancement.

The boundary layer theory for heat and fluid flow is an important and hot topic in applied mathematics and engineering applications. As a matter of fact, the formation of a boundary layer over a solid surface is a common phenomenon in a viscous flow. So, it has been the subject of various researches for decades. Considering heat transfer within the boundary layer of nanofluids, Manjunatha et al. [11], Sharma and Mishra [12], Roy et al. [13], Munir et al. [14], and Bilal et al. [15] addressed the boundary layer flow and heat

transfer flat surfaces. Yasin et al. [16] studied the stagnation point flow and boundary layer heat transfer over a stretching sheet. Rashed et al. [17] utilized a two-phase model to investigated the boundary layer heat transfer of nanofluids over a plate in motion. Madhu et al. [18] investigated the non-Newtonian effects of nanofluids over a stretching sheet. They noticed that the local Nusselt number varies inversely with the power-law index of the non-Newtonian fluid.

Reddy et al. [19] studied the boundary layer heat transfer of nanofluids over an inclined vertical surface. They reported that the nanoscale effects of Brownian motion and thermophoresis tend to increase the plate's boundary layer thickness. Reddy and Chamkha [20] analyzed the natural convection boundary layer heat transfer of nanofluids over a cone in the presence of chemical reactions. The outcomes reveal that the presence of a chemical reaction decreases the amount of the temperature gradient of nanofluid at the surface. However, the boundary layer heat transfer of a suspension of NEPCMs has not been explored yet.

As mentioned, the suspension of a NEPCMs shows promising properties as a heat transfer working fluid. In this regard, several studies addressed the effect of nano/microencapsulation of PCMs in micro channel heat transfer applications. Seyf et al. [21] numerically studied the flow field and thermal performance of a slurry of water-NEPCM over an isothermal unconfined square-cylinder in a channel. The core of the NEPCM was produced from n-octadecane, and the average size of capsules was 100 nm. In another research, Seyf et al. [22] investigated the thermal responses of octadecane NEPCM suspended in polyalphaolefin (PAO) in a microtube heat sink. The results reveal that using NEPCMs considerably enhances the heat transfer rate, while it tremendously increases the pressure drop. They also reported that when the mass-concentration of the nanoparticles increases, the heat transfers more evenly, and it accelerates temperature uniformity. In another numerical investigation conducted by Rehman et al. [23] the thermal enhancement and hydrodynamics characteristics of a confined slot jet impingement for a mixture of NEPCM as a coolant were examined. The water-base coolant was composed 100 nm n-octadecane NEPCM particles. They found that dispersing NEPCM particles in the base fluid resulted in notable enhancement of the thermal performance. However, the presence of NEPCMs also increased the viscosity of the slurry, consequently increasing the pressure drop. In a recent study, Edalatifar et al. [24] employed an artificial intelligence approach to estimate the free convection heat transfer of NEPCMs in an enclosure.

Ho et al. [25] conducted an experiment to inspect the impact of using encapsulated PCMs on the heat transfer enhancement of micro channels. Their report shows up to 52% improvement in heat transfer in some cases. However, in some cases, the possibility of a reduction in heat transfer due to utilizing encapsulated particles is detected. Wang et al. [26] analyzed the thermal performance of encapsulated PCM particles flowing through microchannels. They suggested that using 2% of encapsulated nanoparticles can boost the rate of heat transfer up to 1.36 times higher than that of distilled water when the particles underwent the phase transition. Ho et al. [27, 28] synthesized samples of nanofluids (water-Al2O3 nanofluids) and samples of a slurry of encapsulated PCMs. They examined the thermal performance of the samples in a tube [27] and a mini channel heat sink [28]. The results reveal that the performance of each type of nanofluid or slurry depends on variables such as the flow rate, heat transfer, and the downstream or upstream position.

Although there are noteworthy studies addressing the flow and thermal behavior of NEPCMs in channels, there is no study so far, which explores the motion and thermal behavior of NEPCMs in boundary layer flows. The main goal of the present investigation is to theoretically study the free convection boundary layer flow and heat transfer of NEPCMs over a hot flat plate for the first time.

2. MATHEMATICAL MODEL

Consider a stabilized dilute mixture of NEPMC particles suspended in a pure liquid, which flows over a flat plate forming a boundary layer. These particles are capsules of PCMs comprising a shell layer and a PCM core. The plate is placed in a quiescent suspension of a base fluid and NEPCMs. The plate is at the constant temperature of T_w, and the surrounding fluid is at the cold temperature of T_∞. Fig.1 illustrates the details of the coordinate system and the physical model. The gravity acts in a downward direction. The thermal buoyancy force gives rise to natural convection, which flows across the plate in the upward direction. The transient temperature of NEPCM particles (T_f) is lower than the temperature of the plate, even though it remains above T_∞ the cold ambient temperature. The NEPCMs move with the natural convection flow of the base fluid. When NEPCM particles reach hot regions ($T>T_f$), a part of the thermal energy is absorbed as the latent heat through the phase transition of the nanoparticles from solid to liquid. Accordingly, when they reach cold places ($T<T_f$), they cool down and undergo solidification by releasing their energy.

Due to the significance of heat of transformation, a considerable advance in the convection can be expected by using a suspension of NEPCM nanoparticles. However, the presence of NEPCM particles changes other thermophysical properties of the suspension, including the density, the thermal conductivity, the dynamic viscosity, and the thermal volume expansion of the suspension. Consequently, these thermophysical properties can alter the convection of the suspension. Thus, modeling and systematic inspection of convective heat transfer of NEPCM suspensions are essential to evaluate the thermal behavior of NEPCMs.
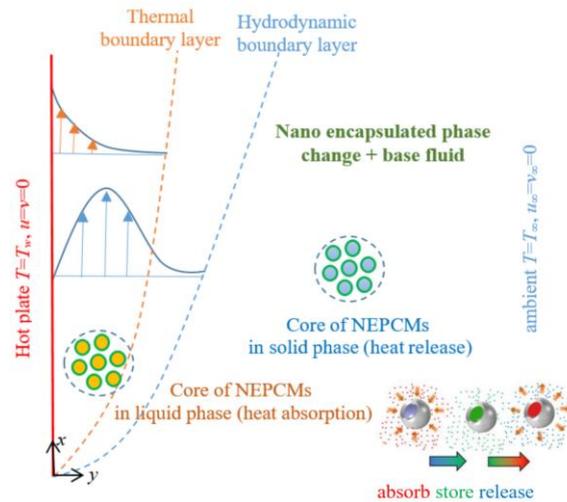

Fig. 1 Schematic view of the physical model and the coordinate system

When it comes to modeling the boundary layer and heat transfer of NEPCMS, considering some presumptions and simplifications is inevitable. In the present study, the deviation of the wall's temperature from ambient is reckoned limited. Hence, aside from density which is modeled using the Boussinesq model and prompts the buoyancy forces, the temperature does not affect the other thermophysical properties. The temperature of the nanoparticles and the fluid around them is the same due to very tiny size of nanoparticle. The volume fraction of

NEPCM particles is considerably small (ϕ), and hence, the suspension of NEPCMs nanoparticles is a dilute suspension, obeying the Newtonian fluid model. Finally, the particles are considered uniformly dispersed within the base fluid, and the suspension remains homogeneous and stable.

By employing the buoyancy effects, the governing equations for the NEPCM's suspension within a base fluid can be introduced as [23, 29]:

$$\frac{\partial u}{\partial x} + \frac{\partial v}{\partial y} = 0, \tag{1}$$

$$\rho_{\text{b}} \left(u \frac{\partial u}{\partial x} \right) + \rho_{\text{b}} \left(v \frac{\partial u}{\partial y} \right) = -\frac{\partial P}{\partial x} + \mu_{\text{b}} \left[\frac{\partial^2 u}{\partial x^2} + \frac{\partial^2 u}{\partial y^2} \right] + g \beta_{\text{b}} \rho_{\text{b}} \left[T - T_{\infty} \right] \tag{2a}$$

$$\rho_{\text{b}} \left(u \frac{\partial v}{\partial x} \right) + \rho_{\text{b}} \left(v \frac{\partial v}{\partial y} \right) = -\frac{\partial P}{\partial y} + \mu_{\text{b}} \left[\frac{\partial^2 v}{\partial x^2} + \frac{\partial^2 v}{\partial y^2} \right] \tag{2b}$$

$$\left(\rho C p \right)_{\text{b}} \left(u \frac{\partial T}{\partial x} \right) + \left(\rho C p \right)_{\text{b}} \left(v \frac{\partial T}{\partial y} \right) = k_{\text{b}} \left[\frac{\partial^2 T}{\partial x^2} + \frac{\partial^2 T}{\partial y^2} \right] \tag{3}$$

where u and v are the velocity components in the x and y directions, respectively. T represents the temperature and P the pressure. In the aforementioned equations, ρ and μ are presenting the density and the dynamic viscosity, respectively. The specific heat capacity (Cp), and the thermal conductivity (k) are also thermal characteristics of the suspension. The gravitational constant is denoted by g, and the coefficient of thermal volume expansion is represented by β. The subscript of b indicates the bulk properties attributed to a suspension of NEPCM fluid. By employing the usual boundary layer approximations, the control equations (1)-(3) are simplified as:

$$\left[\frac{\partial u}{\partial x} + \frac{\partial v}{\partial y} \right] = 0, \tag{4}$$

$$\rho_{\text{b}} \left(u \frac{\partial u}{\partial x} \right) + \rho_{\text{b}} \left(v \frac{\partial u}{\partial y} \right) = -\frac{\partial P}{\partial x} + \mu_{\text{b}} \frac{\partial^2 u}{\partial y^2} + g \beta_{\text{b}} \rho_{\text{b}} \left[T - T_{\infty} \right] \tag{5a}$$

$$\frac{\partial P}{\partial y} = 0 \tag{5b}$$

$$\left(\rho C p \right)_{\text{b}} \left(u \frac{\partial T}{\partial x} \right) + \left(\rho C p \right)_{\text{b}} \left(v \frac{\partial T}{\partial y} \right) = k_{\text{b}} \frac{\partial^2 T}{\partial y^2} \tag{6}$$

Following the representation of the physical model, the appropriate boundary conditions are introduced as:

$$y = 0: \qquad u = v = 0, \quad T = T_{\text{w}} \tag{7a}$$

$$y \to \infty: \ u, v \to 0, \ T \to T_{\infty}. \tag{7b}$$

3. BULK PROPERTIES OF THE SUSPENSION

The thermophysical properties in the governing equations of Eqs. (4-6) with the subscript of b represent the suspension (a mixture of NEPCMs and the pure liquid) thermophysical properties. Thus, some thermophysical models are required to evaluate the thermophysical features of the mixture. Following [30], it is possible to obtain the density of NEPCMs' mixture and the base fluid using:

$$\rho_b = (1-\phi)\rho_f + \phi\rho_p \tag{8}$$

Here, ρ indicates the density, and ϕ represents the nanoparticles concentration. The subscripts of f and p represent the pure liquid and the nanoparticles, respectively.

The NEPCM nanoparticles are consist of a shell and a core PCM [30, 31]. Therefore, the density of NEPCM composed of a shell and a core PCM can be evaluated as [30, 32]:

$$\rho_p = \frac{(1+\iota)\rho_c\rho_s}{\rho_s + \iota\rho_c} \tag{9}$$

where c and s as subscripts indicate the core and the shell, respectively, and ι signifies the weight ratio of the core-shell. In Eq. (9), the density of the core PCM is considered as the mean of its solid and liquid densities. The subscript p also denotes the nanoparticles.

As discussed by Khanafer and Vafai [5], the assumption of thermal equilibrium between the particles and the pure liquid makes it possible to drive the effective heat capacity of both a suspension of nanoparticles and the pure liquid from the energy equations as follow:

$$Cp_b = \frac{(1-\phi)\rho_f Cp_f + \phi\rho_p Cp_p}{\rho_b} \tag{10}$$

However, many of the previous researchers have preferred to use a more simplified relation as [30, 32]:

$$Cp_b = (1-C_m)Cp_f + C_m Cp_p \tag{11}$$

where Cp_p is the specific heat of encapsulated particles. C_m represents the mass fraction of NEPCM particles, which is related to the particles concentration by $\phi = C_m \times \rho_b/\rho_p$ [32]. Here, we use the definition of Eq. (8) for the evaluation of the bulk specific heat capacity of the suspension. When there is no phase transition, Cp_p is calculated using the following relation [32]:

$$Cp_p = \frac{(Cp_{c,l} + \iota Cp_s)\rho_c\rho_s}{(\rho_s + \iota\rho_c)\rho_p} \tag{12}$$

where the core PCM's specific heat capacity ($\underline{Cp}_{c,l}$) can be taken through the mean of its solid and liquid specific heat capacities. Providing that the phase transition is taken into account in evaluating the heat transfer and the latent heat of the confined particle is at hand, it is possible to employ an approximate profile with an integral value equal to the latent heat of phase change. For example, a rectangular, a triangle, or a sinusoidal profile is feasible for modeling the temperature dependent specific heat of encapsulated particles [22, 30, 33, 34]:

$$Cp_c = Cp_{c,l} + \frac{h_{sf}}{T_{Mr}} \qquad (13a)$$

$$Cp_c = Cp_{c,l} + \left(\left[\frac{h_{sf}}{T_{Mr}} - Cp_{c,l} \right] \frac{\pi}{2} \sin \left[\frac{T-T_1}{T_{Mr}} \pi \right] \right) \qquad (13b)$$

$$Cp_c = Cp_{c,l} + 2(T-T_1) \left[\frac{h_{fs}}{T_{Mr}^2} - \frac{Cp_{c,l}}{T_{Mr}} \right] \qquad (13c)$$

where T_{Mr} is the phase-change temperature range ($T_{Mr} = T_2 - T_1$). Indeed, the phase change takes place in the range of T_1 to T_2 instead of the exact fusion temperature of T_f. Taking the fusion temperature as the middle of the transition temperature range, T_1 and T_2 can be introduced as $T_1 = T_f - T_{Mr}/2$ and $T_2 = T_f + T_{Mr}/2$. In the case of temperatures out of the melting range, the magnitude of the specific heat of the nanoparticle is matching Cp_c, and regarding temperatures within the range, the specific heat of the particle is estimated to solve the aforementioned equation. Here, following the literature studies [22, 30, 33, 34], it is presumed that the specific heat of the molten and the solid PCM is similar. As stated by Alisetti and Roy [34], the divergence between applying different profiles for evaluation of the specific heat of PCM in a circular duct is under 4%. Thus, in the present study, the simple rectangle profile of Eq. (11a) is employed to be a representative of the latent heat of NEPCM as a function of temperature. As a result, by considering the phase change latent heat capacity and the sensible heat capacity, the total heat capacity of the suspension of NEPCM capsule can be evaluated as:

$$Cp_p = \frac{(Cp_c + \iota Cp_s) \rho_c \rho_s}{(\rho_s + \iota \rho_c) \rho_p} \qquad (14a)$$

where

$$Cp_c = Cp_{c,l} + \begin{cases} 0 & T < T_1 \\ \dfrac{h_{sf}}{T_{Mr}} & T_1 < T < T_2 \\ 0 & T > T_2 \end{cases} \qquad (14b)$$

The coefficient of the thermal volume expansion, β_p, is evaluated through the upcoming equation, which was discussed by Khanafer and Vafai [5] for a base fluid containing nanoparticles:

$$\beta_b = (1-\phi)\beta_f + \phi\beta_p \qquad (15)$$

Now, closure models for the estimation of the dynamic viscosity and the thermal conductivity of the suspension are required. Many of the previous studies have evaluated the thermal conductivity of Micro/Nano-EPCM as two parts of static and dynamic thermal conductivity. In most of the literature-works, the mixture's static thermal conductivity was estimated by using the Maxwell model [5, 35], and then the dynamic thermal conductivity of the mixture was modeled using the fluid shear rates [22, 29, 30, 36]. However, Buongiorno [37], using a scale analysis approach, demonstrated that the shear rate effects are not of importance in the nanoscales. Hence, it can be concluded that the thermal conductivity

relations for the microencapsulated PCMs are not applicable to the case of nano-encapsulated suspensions. In most of the literature studies, the dynamic viscosity of the suspension of Micro-Encapsulated PCMs (MEPCMs) was approximated using the Vand [38] model as [22, 30]:

$$\frac{\mu_b}{\mu_f} = \left(1 - \phi - A\phi^2\right)^{-2.5} \tag{16}$$

In Eq. (16), the parameter of A depends on the size of particles and can be evaluated using a curve-fitting on the experimental data. For example, the value of A has been reported as A=1.16 for 0.13mm diameter glass spheres [38], A=3.4 (10–30 μm diameter MEPCM particles) [39], A=3.7 (6.3μm average diameter) [40], and A=4.45 (about 10 μm diameter MEPCM particles) [41]. It should be noted that the model of Vand [35] has been introduced for the MEPCM particles and not for Nano-EPCM particles.

Regarding nanoparticles, Buongiorno [42] and Venerus et al. [43] addressed the effects that the presence of nanoparticles can lay upon the dynamic viscosity and the thermal conductivity of dilute suspensions of nanofluids in two comprehensive benchmark studies. More than thirty authors around the world have studied the aforementioned properties of nanofluids in different experimental setups and through various types of measurement devices. The outcomes demonstrate the possibility of expressing the dynamic viscosity and the thermal conductivity of fluids containing nanometer-sized particles by linear relations. Following this outcome, Ghalambaz et al. [44] utilized the upcoming linear equations to study the heat and mass transfer of nanofluids:

$$\left(\frac{k_b}{k_f}\right) = \left[1 + Nc\phi\right] \tag{17a}$$

$$\left(\frac{\mu_b}{\mu_f}\right) = \left[1 + Nv\phi\right] \tag{17b}$$

Here Nc is the thermal-conductivity number, and Nv indicates the dynamic-viscosity number. The magnitudes of Nc and Nv depend on several parameters, including the shape of the particles, the nanoparticles material, the pure liquid, and the operating temperature [44]. It is obvious that the higher the value of Nc or Nv, the greater the amplification of the thermal conductivity or the dynamic viscosity when the flow contains nanoparticles.

Nc and Nv are attainable by applying linear curve fitting over gathered experimental data for the suspensions thermophysical properties. A list of values of Nc and Nv is evaluated and reported in [44]. It is noteworthy to mention that these relations are valid for a diluted suspension of nanoparticles, and more advance relations or actual experimental data shall be used for high volume fractions of nanoparticles. Here, Eqs. (17a) and (17b) are adopted to determine the thermal conductivity of the suspension and the dynamic viscosity within the flow field.

4. SIMILARITY SOLUTION

For the purpose of transforming the equations governing the boundary layer flow field along with the attributed boundary conditions into a selection of ordinary differential equations, some similarity variables are required to be proposed. First, in order to satisfy

the continuity equation, the stream function is introduced into it as $u=\partial\psi/\partial y$ and $v=-\partial\psi/\partial x$. The pressure between equations of (2a) and (2b), is excluded between momentum equations in x-direction and y-direction by taking the cross. For obtaining a similarity solution through which the equations can be rearranged as a scaled expression, the similarity variables are proposed as:

$$\eta = \frac{y}{x}\text{Ra}_x^{\frac{1}{4}} \tag{18a}$$

$$S = \frac{\psi}{\alpha\,\text{Ra}_x^{\frac{1}{4}}}, \qquad \theta = \frac{T-T_\infty}{T_w-T_\infty} \tag{18b}$$

where η is the similarity variable, S and θ are the scaled flow and temperature. Here, the local Rayleigh number (Ra_x) is introduced as:

$$\text{Ra}_x = \frac{\rho_f\, g\beta_f\left(T-T_\infty\right)x^3}{\mu_f\alpha_f} \tag{19}$$

By positioning the similarity variables of Eq. (18) and using the thermal conductivity and dynamic viscosity relations of Eq. (17), the partial differential equations of Eqs. (5) and (6) along with the boundary conditions of Eq. (7) are explained into a series of non-linear ordinary differential equations as:

$$\frac{1}{4\,\text{Pr}}\left(2S'S'-3S\,S''\right) = \frac{\rho_f}{\rho_b}\left(1+Nv\phi\right)S''' + \frac{\rho_f}{\rho_b}\frac{\beta_b}{\beta_f}\theta \tag{20}$$

$$\left(1+Nc\phi\right)\theta'' + \frac{3}{4}\frac{\left(\rho c\right)_b}{\left(\rho c\right)_f}S\theta' = 0 \tag{21}$$

where $\text{Pr}=\mu_f/(\rho_f\,\alpha_f)$. The density ratio of ρ_b/ρ_f can be simply evaluated using Eq. (7) as $(1-\phi)+\phi\rho_p/\rho_f$. The thermal expansion ratio of β_b/β_f can be rewritten as $\phi\beta_p/\beta_f+(1-\phi)$ by using Eq. (15). The other important thermophysical property would be the heat capacity ratio $(\rho Cp)_b/(\rho Cp)_f$ which is evaluated using Eqs. (8), (10) and (14) as follow:

$$\frac{\left(\rho Cp\right)_b}{\left(\rho Cp\right)_f} = \left(1-\phi\right) + \lambda\phi + \frac{1}{\delta Ste}f\,\phi \tag{22}$$

where θ_f represents the phase-change temperature, δ is the parameter of fusion range, which should be a very small number. When δ approaches zero, the phase change temperature approaches the scaled phase change temperature. λ is the scaled heat capacity introduced as the proportion of the sensible heat capacity of NEPCM nanoparticles to the sensible thermal capacity of the base fluid, where Ste is the Stefan number. These scaled parameters and numbers are introduced as:

$$\theta_f = \frac{T_f-T_\infty}{\left(T_w-T_\infty\right)}\ \delta = \frac{T_{Mr}}{\left(T_w-T_\infty\right)},\ \lambda = \frac{\left(Cp_{c,l}+\iota Cp_s\right)\rho_c\rho_s}{\left(\rho Cp\right)_f\left(\rho_s+\iota\rho_c\right)},$$

$$Ste = \frac{\left(\rho Cp\right)_f\left(T_w-T_\infty\right)\left(\rho_s+\iota\rho_c\right)}{h_{sf}\rho_c\rho_s} \tag{23}$$

and
$$f = 1 \ if \left(\theta_f - \frac{\delta}{2} < \theta < \theta_f + \frac{\delta}{2} \right) \qquad \text{otherwise} \qquad f = 0 \qquad (24)$$

By substituting the final scaled form of the thermo-physical ratio parameters, the governing equations of the flow and heat transfer are rewritten as:

$$\frac{1}{4 \Pr} \left((1-\phi) + \phi \frac{\rho_p}{\rho_f} \right) (2S'S' - 3SS'') = (1 + Nv\phi) S''' + \left((1-\phi) + \phi \frac{\beta_p}{\beta_f} \right) \theta \qquad (25)$$

$$(1 + Nc\phi) \theta'' + \frac{3}{4} \left((1-\phi) + \lambda \phi + \frac{1}{\delta Ste} f \phi \right) S\theta' = 0 \qquad (26)$$

In the above equations, it should be noticed that f is not a constant, and it a function of scaled temperature as defined by Eq. (24). The transformed form of the boundary conditions of Eq. (7) are:

$$at \ \eta = 0: \qquad S(0) = 0, \qquad S'(0) = 0, \qquad \theta(0) = 1, \qquad (27a)$$

$$as \ \eta \to \infty: \qquad S'(\eta) \to 0, \qquad \theta(\eta) \to 0. \qquad (27b)$$

The important characteristics of heat transfer of the NEPCMs suspension are the heat transfer at the surface. The balance in the heat transfer at the surface of the plate is given using the convective heat transfer coefficient (h) as:

$$-k_b \frac{\partial T}{\partial y} = h(T_w - T_\infty) \qquad (28)$$

The local Nusselt number is achieved through using the above equation and implementing the similarity variables brought in Eq. (18), and equals to:

$$Nu_x = -\frac{k_b}{k_f} \theta'(0) \mathrm{R} a_x^{\frac{1}{4}} \qquad (29)$$

where, using Eq. (17a), the local Nusselt number can be rewritten as:

$$\mathrm{Nu}_x \mathrm{Ra}_x^{-\frac{1}{4}} = -(1 + Nc\phi) \theta'(0) \qquad (30)$$

It is worth noticing that the term $Nu_x Ra_x^{-1/4}$ is known as the reduced Nusselt number (Nur).

5. NUMERICAL METHOD AND CODE VALIDATION

Eqs. (25) and (26) are a set coupled, high order, and non-linear ordinary differential equations. It is very hard to obtain an analytical solution for non-linear high-order differential equations. Hence, a numerical approach is required to integrate the equations. Here, bvp4c finite element code with automatic grid adaptation and error control is employed for the purpose of finding a solution for the governing equations along with the boundary conditions. In order to implement the ODE equations in bvp4c code, they need to be written in the form of a set of first-order coupled equations as follow:

$$y_1' = y_2, \quad y_2' = y_3, \quad y_3' = \frac{\frac{1}{4\Pr}\left((1-\phi)+\phi\frac{\rho_p}{\rho_f}\right)\left(2y_2^2 - 3y_1 y_3\right) - \left((1-\phi)+\phi\frac{\beta_p}{\beta_f}\right)y_4}{(1+Nv\phi)},$$

$$y_4' = y_5, \quad y_5' = -\frac{3}{4}\frac{\left((1-\phi)+\lambda\phi+\frac{1}{\delta Ste}f\phi\right)y_1 y_5}{(1+Nc\phi)}$$

(31)

$$f = 1 \quad if\left(\theta_f - \frac{\delta}{2} < y_5 < \theta_f + \frac{\delta}{2}\right) \quad \text{otherwise} \qquad f = 0 \tag{32}$$

Accordingly, the corresponding boundary conditions using the new notation are:

$$\eta = 0: \qquad y_1(0) = 0, \qquad y_2(0) = 0, \qquad y_4(0) = 1, \tag{33a}$$

$$\eta \to \infty: \qquad y_2(\eta) \to 0, \quad y_4(\eta) \to 0. \tag{33b}$$

Two of the boundary conditions are approaching infinity. Therefore, the governing equations have to be solved in a large domain to reach an asymptotic solution. In the present study, the value of η_∞ is increased starting from $\eta_\infty = 10$ to higher values, and the reduced Nusselt number is monitored to ensure that the asymptotic solution is reached and it is independent of the selected value of η_∞. The absolute error was set as 10-8, and the absolute relative error was set as 10^{-6}. More details about the utilized code can be found in [45].

The reliability of the present code is evaluated by comparing the obtained results with the literature. In Fig. 2 the temperature profiles brought by Bejan [46] are compared with those reported in the present research.
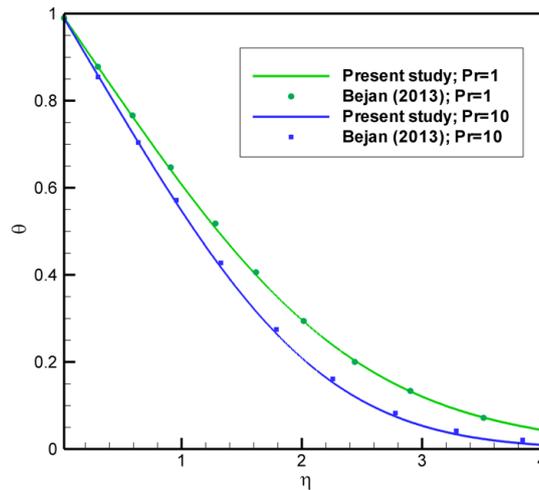

Fig. 2 A comparison between the current data and those of Bejan [46]

Table 1 shows a comparison between the outcomes of the present study and the results that can be found in the literature for the reduced Nusselt number (Nur) when $\phi=0$.

Table 1 Comparison Nur calculated in the present investigation and the results available in literature when $\phi=0$

Pr	Present study	Bejan [46]
0.72	0.3874	0.387
1	0.4010	0.401
2	0.4260	0.426
10	0.4650	0.465
100	0.4900	0.490

6. RESULTS AND DISCUSSION

Here, for estimating the range of the scaled parameters, n-octadecane [47] for the core PCM, poly (methyl methacrylate) PMMA for the shell [48], and water for the base fluid [47] are adopted. The core-shell weight proportion is selected as $\iota=0.7$. In this case, λ and Ste (Stefan number) can be approximated as 0.4 and 0.313, respectively. The volume fraction of the NEPCM nanoparticles within the water is adopted to be fixed as $\phi=5\%$.

The fusion temperature is picked in the range of $0<\theta_f<1$ where the scaled ambient temperature and the scaled hot wall temperature equal to zero and unity, respectively. To illustrate the results, the scaled parameters are adopted in the following range: $0<Nc<6$ and $0<Nv<6$ for a mixture where nanoparticles are distributed throughout a base fluid. Since the PCM core is less dense than water [49, 50], the density ratio is implemented as $\rho_p/\rho_f=0.9$, and the buoyancy ratio of $\phi\times\beta_p/\beta_f$ is assumed negligible because of the inconsiderable volume fraction of nanoparticles (0.05) and very low thermal expansion of solid particles compared to a liquid. The Prandtl number (Pr) is fixed 6.2, which is about the Prandtl number of water. For a fixed value of Pr=6.2, the asymptotic value of η_∞ is about $\eta_\infty=20$. As a summary, the preset values of the scaled parameters would be assigned as Pr=6.2, $\theta_f=0.2$, $\iota=0.7$, $\lambda=0.4$, $Ste = 0.313$, $Nc=Nv=3.0$, $(\rho_p/\rho_f)=0.9$, and $(\phi\times\beta_p/\beta_f)=0$. In this study, the results are presented as the preliminary values of the scaled parameters, and in other circumstances, the value of the parameter will be stated.

For the first part of the numerical calculations, it is examined how the average Nusselt number may vary by the changes in the value of δ. The Delta parameter (δ) is the scaled fusion range, and it should be a small parameter. The calculations for various values of δ were carried out. The outcomes indicate that the results are independent of this parameter for $\delta<0.025$. It is important to keep in mind that very small values of δ lead to a very low fusion temperature range. Since the latent heat of phase change varies according to a temperature within the fusion process, the quality of the utilized grid is of utmost importance for capturing the phase change within acceptable accuracy. The utilized bvp4c code in the present study enjoys the advantage of automatic error control and automatic grid adaptation. Although the automatic error control and automatic grid adaptation can significantly reduce the computational cost of the calculations to deal with a small value of δ, using a small value of δ results in a dramatical increase of computational costs. Hence, for the sake a balance between the accuracy and computational cost, the appropriate value of $\delta=0.025$ is adopted for the calculations.

Since all of the presented results are derived from scaled governing equations, the scaled suffix is left out for brevity. Figures 3 and 4 depict the effect of the fusion temperature (θ_f) on the velocity and temperature profiles. The computational domain of solution is about η_∞=20; however, here, the results are plotted in a smaller domain for the sake of graphical clarity. As mentioned, the velocity profiles equal to zero at the surface and tend to zero at the infinity, which satisfies the hydrodynamic boundary conditions. There is a maximum velocity peak next to the heated surface. Any rise in the phase-change temperature elevates the maximum value of the maximum-velocity peak. It also shifts the maximum-velocity peak to the right. Attention to the temperature profiles of Fig. 4 illustrates that when the fusion temperature rises, the temperature gradient dwindles. Moreover, in the case of θ_f=0.1, a sharp change in the path of the temperature profile can be observed at the location of about η=2.4. The similar trends of the path changes but smoother can be seen for other fusion temperature profiles. The surge of the fusion temperature shifts the mentioned path changes towards the surface. Indeed, the location of this path change is the place that the change phase of the NEPCM particles occurs. In the case of θ_f=0.1, the path change occurs at η=2.4 corresponding to the temperature of θ=0.1. Indeed, when the fusion temperature elevates, the magnitude of the temperature profile extends. Consequently, the increase in temperature corresponds to the increase of the buoyancy forces. Hence, as it was observed in Fig. 3, the elevation of the fusion temperature promotes the fluid velocities and the maximum-velocity peaks. The reason behind the shift of the maximum-velocity peaks toward the surface (by the rise in the fusion temperature) is that the velocity profiles and the buoyancy forces tend to follow the trend of the change path in the temperature profiles due to the growth of the transient temperature. As mentioned, a surge of the fusion temperature shifts the temperature profiles toward the hot plate.
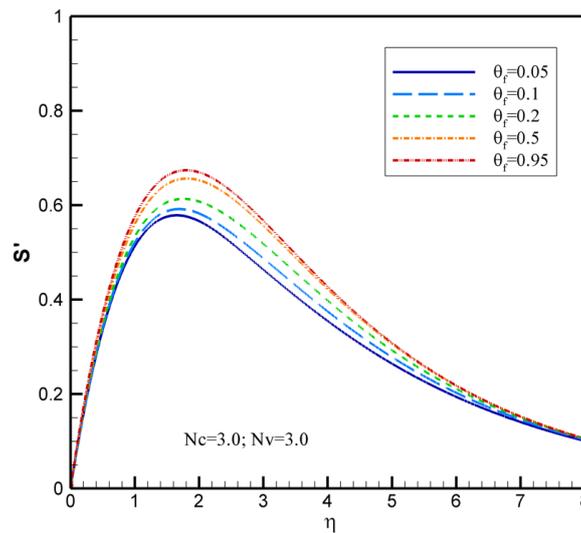

Fig. 3 The velocity profiles for various values of the scaled fusion temperature (θ_f) when $Nc=Nv$=3.0
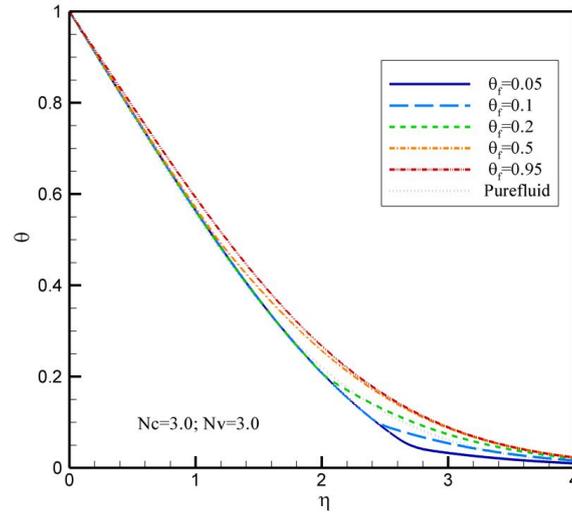
Fig. 4 The temperature profiles for various values of the scaled fusion temperature (θ_f) when $Nc=Nv=3.0$

Figures 5 and 6 show the effect of fusion temperature (θ_f) and the thermal conductivity number (Nc) and the dynamic viscosity number (Nv) on the magnitude of the temperature gradient and the reduced Nusselt number at the wall surface. For each set of Nc and Nv numbers, Fig. 5 shows that there is a maximum-peak for the temperature gradient about $\theta_f=0.2$. Starting from a low value of $\theta_f \sim 0.025$, the temperature gradient and Nusselt number raise by the increase of θ_f until about $\theta_f=0.2$, which corresponds to a peak for the maximum temperature gradient. After that, whenever the fusion temperature (θ_f) ascends, the Nusselt number and the temperature gradient follow a descending trend. A smooth local-minimum can be seen about $\theta_f = 0.975$. In fact, the growth of the fusion temperature physically means that the phase transition at the core of nanoparticles will occur in a temperature closer to the wall temperature. When the fusion temperature and the wall temperature are close to each other, the NEPCM particle undergoes phase change just next to the wall, and hence, it would keep the temperature of the liquid at a high level next to the wall. However, it should be heeded that the phase transition occurs, a substantial amount of energy would be absorbed because of the latent heat of the phase change, which results in the increase of the heat transfer rate. Consequently, when the phase changes next to the wall, the wall temperature gradient decreases, which eventually drops the magnitude of heat transfer enhancement. Although this transition next to the wall declines the wall temperature gradient, still the other thermophysical properties, including the enhancement of conduction, can result in an overall improvement of the heat transfer in the presence of NEPCM particles. Hence, as seen in Fig. 6, generally, the heat transfer rate is higher within the NEPCM suspension than the pure fluid. The Nusselt number of a pure base fluid with no NEPCM particle is depicted as a gray narrow dashed line in Fig. 6.
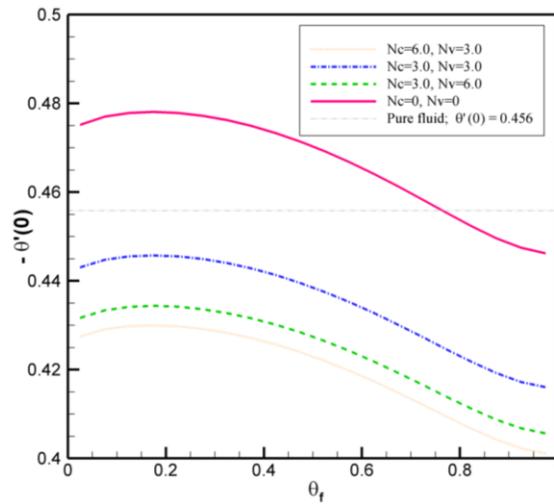
Fig. 5 The surface temperature gradient vs the scaled fusion temperature (θ_f) and for different Nc and Nv
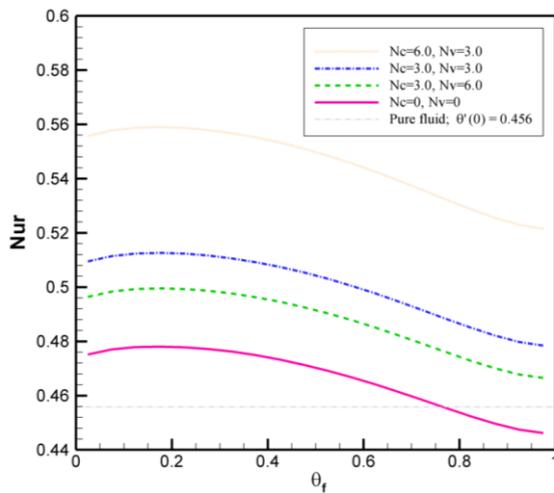

Fig. 6 The reduced Nusselt vs the scaled fusion temperature (θ_f) and for different Nc and Nv

At very low fusion temperatures, the phase of NEPCM particles changes at the boundary layer's edge, which is quite far from the hot surface. A small increase in the fusion temperature shifts the phase transition of the nanoparticles inside the boundary layer, which leads to an increase in the heat capacity of the cold fluid at a cool temperature. As it was observed in Fig. 4, as an example for θ_f=0.1, the phase transition occurs at η=2.4. It was also observed that any rise in the fusion temperature (θ_f) would shift the phase change of NEPCM particles towards the wall. The phase change tends to uniform the temperature profiles about the fusion temperature. So, when it occurs with a sufficient distance from the

wall, indeed it decreases the actual the thermal boundary layer's thickness, and the hot wall sees a uniform cold region in nearby. This is where the higher fusion temperature improves the reduced Nusselt number.

Attention to the case of $Nc=Nv=0$ in Figs. 5 and 6 show that the temperature gradient and Nusselt number are higher than the pure fluid (the gray line) in most cases. The case of $Nc=Nv=0$ indeed neglects the major effect of the increment of thermal conductivity and dynamic viscosity of the NEPCM suspension because of existing particles. In this case, only the thermal capacity ratio, the density ratio, and the buoyancy ratio parameters remain effective. In these figures, it is obvious that the heat transfer of NEPCM suspension is higher than the pure fluid for the case of $\theta_f<0.8$. However, for the fusion temperature higher than 0.8, the heat transfer would be less than that of the pure fluid since the phase transition affects the surface temperature gradient.

The change of Nc and Nv only shifts the observed trend of behavior for temperature gradient and Nusselt number. The growth of the thermal conductivity (Nc) number declines the magnitude of the temperature gradient but boosts the Nusselt number. Indeed, when Nc increases, the thermal conductivity of the suspension surges in the presence of NEPCM particles. The increase of conduction tends to uniform the temperatures next to the wall, which causes a drop of the temperature gradient. However, the heat transfer can be calculated as the thermal conductivity multiple by the temperature gradient. Hence, although the magnitude of the temperature gradient of the surface drops, a better thermal conductivity would boost the overall heat transfer rate.

Following any rise in the dynamic viscosity (Nv) number, the suspension's viscosity in the presence of the particles grows, and the rate of heat the flow accordingly plummets. The increase of viscosity would diminish the fluid velocity, and as a consequence, the overall rate of heat transfer. Based on the results of Fig. 6, improvement in the heat transfer is expected in most cases of regular suspensions of NEPCM particles. Fig. 7 depicts the reduced Nusselt number as a function of Stefan number. As seen, the increase of Stefan number reduces the thermal performance of NEPCMs. It should be pointed out that the phase transition's latent heat is reversely related to Stefan number. This means that a large value of Stefan number represents a very low latent heat of phase change, and in contrast, a small value of Stefan number indicates a large amount of latent heat of phase change. Fig. 7 reveals that NEPCM particles with low Stefan number are very effective on the increase of heat transfer. It also confirms that not only the Stefan number of NEPCM particles but also the fusion temperature of NEPCM particles are important. At fusion temperatures close to the hot wall temperature, the presence of NEPCM particles only shows a minor enhancement in heat transfer rate regardless of the Stefan number.

Table 2 lists a brief summary of the impact of the scaled parameters on the amount of the temperature and the velocity gradients at the wall. Adopting the first row of the table as a reference and comparing the results of the other rows with this row, Table 2 shows that the magnitude of the wall temperature gradient ($-\theta'(0)$) is a decreasing function of λ, θ_f, and Ste. The effect of the variation of the density ratio (ρ_p/ρ_f) is negligible. The surface velocity gradient is a degreasing function of λ and (ρ_p/ρ_f) and an increasing function of θ_f and Ste.
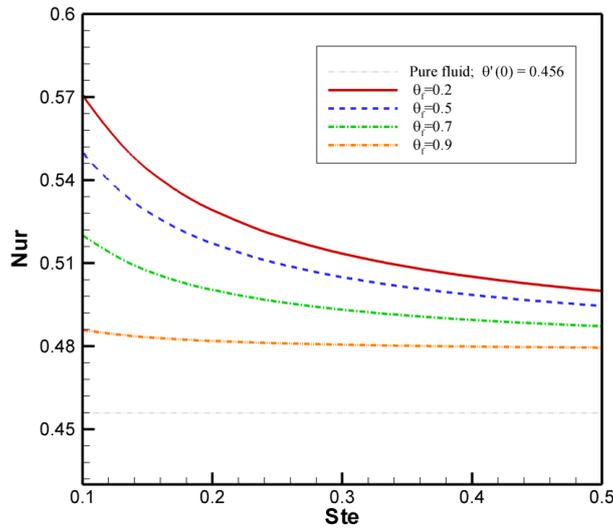
Fig. 7 The reduced Nusselt number vs Stefan number for various scaled fusion temperatures (θ_f)

Table 2 The magnitude of temperature gradient ($-\theta'(0)$) and the velocity gradient ($S''(0)$) for various value of scaled parameters when ϕ=0.05, $(\phi \times \beta_p/\beta_f)$~0, and $Nv=Nc$=3.0

Ste	λ	θ_f	(ρ_p/ρ_f)	$-\theta'(0)$	$S''(0)$
0.3	0.4	0.2	0.9	0.4469	0.8823
0.3	0.4	0.2	0.8	0.4469	0.8825
0.3	0.3	0.2	0.9	0.4463	0.8830
0.3	0.4	0.3	0.9	0.4456	0.8931
0.3	0.4	0.1	0.9	0.4464	0.8696
0.2	0.4	0.2	0.9	0.4606	0.8640

7. CONCLUSIONS

The flow and heat transfer behavior of NEPCM particles dispersed in a pure fluid along a heated vertical plate was studied. The boundary layer governing equations were introduced and rearranged as a group of non-linear ordinary differential equations and solved numerically. The influence of some important scaled parameters, including Prandtl number (Pr), Stefan number (Ste), dynamic viscosity number (Nv), thermal conductivity number (Nc), and fusion temperature (θ_f), as well as density ratio of the NEPCM (ρ_p/ρ_f), were investigated, as summarized below:

- Generally, the presence of NEPCM nanoparticles enhances the natural convection.
- The decrease in the Stefan number enhances the heat transfer rate.
- At the optimum scaled fusion temperature, θ_f ~0.2, the heat transfer rate reaches its maximum value. At $\theta_f = 0.2$, the reduced Nusselt number is increased from Nur=0.445 for the case of the base fluid to 0.56 at 5% Vol. of NEPCM particles, showing 25% enhancement in heat transfer.

▪ As the fusion temperature elevates, the velocities of the NEPCM within the boundary layer rises as well, which, however, does not always lead to the enhancement of heat transfer. For instance, the velocity corresponding to the case of θ_f=0.2 is lower than that of θ_f=0.5, but corresponding to a large heat transfer enhancement. This indicates the significance of how the latent heat of NEPCM particles can affect the heat transfer behavior of suspension.

It shall be noted that one assumption made in this work is that the suspension of NEPCM is diluted (i.e., ϕ<5%). Hence, the interactions among the NEPCM particles and the non-Newtonian effects were neglected. It was also assumed that NEPCM particles remain homogeneous in the fluid. However, in practice, some slip mechanisms such as the Brownian motion and thermophoresis effects could change the local concentration of NEPCM particles, and a suspension with a high volume-fraction of NEPCM particles may behave like slurries. The slip mechanisms of NEPCM particles and non-Newtonian effects should be the subject of future studies.

REFERENCES

1. Fokaides, P.A., Kylili, A., Kalogirou, S.A., 2015, *Phase change materials (PCMs) integrated into transparent building elements: a review*, Materials for renewable and sustainable energy, 4(2), 6.
2. Huang, X., Alva, G., Jia, Y., Fang, G., 2017, *Morphological characterization and applications of phase change materials in thermal energy storage: A review*, Renewable and Sustainable Energy Reviews, 72, pp. 128-145.
3. Moreno, P., Solé, C., Castell, A., Cabeza, L.F., 2014, *The use of phase change materials in domestic heat pump and air-conditioning systems for short term storage: A review*, Renewable and Sustainable Energy Reviews, 39, pp. 1-13.
4. Angayarkanni, S., Philip, J., 2015, *Review on thermal properties of nanofluids: Recent developments*, Advances in colloid and interface science, 225, pp. 146-176.
5. Khanafer, K., Vafai, K., 2011, *A critical synthesis of thermophysical characteristics of nanofluids*, International Journal of Heat and Mass Transfer, 54(19-20), pp. 4410-4428.
6. Liu, C., Rao, Z., Zhao, J., Huo, Y., Li, Y., 2015, *Review on nanoencapsulated phase change materials: preparation, characterization and heat transfer enhancement*, Nano Energy, 13, pp. 814-826.
7. Ghasemi, K., Tasnim, S., Mahmud, S., 2022, *PCM, nano/microencapsulation and slurries: A review of fundamentals, categories, fabrication, numerical models and applications*, Sustainable Energy Technologies and Assessments, 52, 102084.
8. Sarkar, S., Mestry, S., Mhaske, S., 2022, *Developments in phase change material (PCM) doped energy efficient polyurethane (PU) foam for perishable food cold-storage applications: A review*, Journal of Energy Storage, 50, 104620.
9. Sidik, N.A.C., Kean, T.H., Chow, H.K., Rajaandra, A., Rahman, S., Kaur, J., 2018, *Performance enhancement of cold thermal energy storage system using nanofluid phase change materials: a review*, International Communications in Heat and Mass Transfer, 94, pp. 85-95.
10. Shah, K.W., 2018, *A review on enhancement of phase change materials-A nanomaterials perspective*, Energy and buildings, 175, pp. 57-68.
11. Manjunatha, S., Puneeth, V., Gireesha, B.,Chamkha, A., 2021, *Theoretical Study of Convective Heat Transfer in Ternary Nanofluid Flowing past a Stretching Sheet*, Journal of Applied and Computational Mechanics, 8(4), pp. 1279-1286.
12. Sharma, R., Mishra, S., 2020, *Metal and Metallic Oxide Nanofluid over a Shrinking Surface with Thermal Radiation and Heat Generation/Absorption*, Journal of Applied and Computational Mechanics, 8(2), pp. 557-565.
13. Roy, N.C., Hossain, M.A., Pop, I., 2021, *Analysis of Dual Solutions of Unsteady Micropolar Hybrid Nanofluid Flow over a Stretching/Shrinking Sheet*, Journal of Applied and Computational Mechanics, 7(1), pp. 19-33.

14. Munir, S., Maqsood, A., Farooq, U., Hussain, M., Siddiqui, M.I., Muhammad, T., 2022, *Numerical analysis of entropy generation in the stagnation point flow of Oldroyd-B nanofluid*, Waves in Random and Complex Media, doi:10.1080/17455030.2021.2023782.

15. Bilal, M., Ayed, H., Saeed, A., Brahmia, A., Gul, T., Kumam, P., 2022, *The parametric computation of nonlinear convection magnetohydrodynamic nanofluid flow with internal heating across a fixed and spinning disk*, Waves in Random and Complex Media, doi: 10.1080/17455030.2022.2042621.

16. Yasin, M.H.M., Ishak, A., Pop, I., 2015, *MHD stagnation-point flow and heat transfer with effects of viscous dissipation*, *Joule heating and partial velocity slip*, Scientific reports, 5(1), 17848.

17. Rashed, A.S., Mahmoud, T.A., Kassem, M.M., 2021, *Behavior of Nanofluid with Variable Brownian and Thermal Diffusion Coefficients Adjacent to a Moving Vertical Plate*, Journal of Applied and Computational Mechanics, 7(3), pp. 1466-1479.

18. Madhu, M., Kishan, N., Chamkha, A., 2016, *Boundary layer flow and heat transfer of a non-Newtonian nanofluid over a non-linearly stretching sheet*, International Journal of Numerical Methods for Heat & Fluid Flow, 26(7), pp. 2198-2217.

19. Reddy, P.S., Chamkha, A.J., Al-Mudhaf, A., 2017, *MHD heat and mass transfer flow of a nanofluid over an inclined vertical porous plate with radiation and heat generation/absorption*, Advanced Powder Technology, 28(3), pp. 1008-1017.

20. Reddy, P.S., Chamkha, A., 2017, *Heat and mass transfer analysis in natural convection flow of nanofluid over a vertical cone with chemical reaction*, International Journal of Numerical Methods for Heat & Fluid Flow, 27(1), pp. 2-22.

21. Seyf, H.R., Wilson, M.R., Zhang, Y., Ma, H., 2014, *Flow and heat transfer of nanoencapsulated phase change material slurry past a unconfined square cylinder*, Journal of heat transfer, 136(5), 051902.

22. Seyf, H.R., Zhou, Z., Ma, H., Zhang, Y., 2013, *Three dimensional numerical study of heat-transfer enhancement by nano-encapsulated phase change material slurry in microtube heat sinks with tangential impingement*, International journal of heat and mass transfer, 56(1-2), pp. 561-573.

23. Mohib Ur Rehman, M., Qu, Z.G., Fu, R.P., 2016, *Three-dimensional numerical study of laminar confined slot jet impingement cooling using slurry of nano-encapsulated phase change material*, Journal of Thermal Science, 25(5), pp. 431-439.

24. Edalatifar, M., Tavakoli, M.B., Setoudeh, F., 2021, *A Deep Learning Approach to Predict the Flow Field and Thermal Patterns of Nonencapsulated Phase Change Materials Suspensions in an Enclosure*, Journal of Applied and Computational Mechanics, 8(4), pp. 1270-1278.

25. Ho, C.J., Chen, W.C.,Yan, W.M., 2013, *Experimental study on cooling performance of minichannel heat sink using water-based MEPCM particles*, International communications in heat and mass transfer, 48, pp. 67-72.

26. Wang, Y., Chen, Z., Ling, X., 2016, *An experimental study of the latent functionally thermal fluid with micro-encapsulated phase change material particles flowing in microchannels*, Applied Thermal Engineering, 105, pp. 209-216.

27. Ho, C.J., Huang, J., Tsai, P., Yang, Y.M., 2011, *Water-based suspensions of Al2O3 nanoparticles and MEPCM particles on convection effectiveness in a circular tube*, International Journal of Thermal Sciences, 50(5), pp. 736-748.

28. Ho, C.J., Chen, W.C.,Yan, W.M., 2014, *Correlations of heat transfer effectiveness in a minichannel heat sink with water-based suspensions of Al2O3 nanoparticles and/or MEPCM particles*, International Journal of Heat and Mass Transfer, 69, pp. 293-299.

29. Kuravi, S., Kota, K.M., Du, J., Chow, L.C., 2009, *Numerical investigation of flow and heat transfer performance of nano-encapsulated phase change material slurry in microchannels*, Journal of heat transfer, 131(6), 062901.

30. Chai, L., Shaukat, R., Wang, L., Wang, H.S., 2018, *A review on heat transfer and hydrodynamic characteristics of nano/microencapsulated phase change slurry (N/MPCS) in mini/microchannel heat sinks*, Applied Thermal Engineering, 135, pp. 334-349.

31. Du, X., Fang, Y., Cheng, X., Du, Z., Zhou, M.,Wang, H., 2018, *Fabrication and characterization of flame-retardant nanoencapsulated n-octadecane with melamine–formaldehyde shell for thermal energy storage*, ACS Sustainable Chemistry & Engineering, 6(11), pp. 15541-15549.

32. Chen, B., Wang, X., Zeng, R., Zhang, Y., Wang, X., Niu, J., Li, Y., Di, H., 2008, *An experimental study of convective heat transfer with microencapsulated phase change material suspension: laminar flow in a circular tube under constant heat flux*, Experimental Thermal and Fluid Science, 32(8), pp. 1638-1646.

33. Rajabifar, B., 2015, *Enhancement of the performance of a double layered microchannel heatsink using PCM slurry and nanofluid coolants*, International Journal of Heat and Mass Transfer, 88, pp. 627-635.

34. Alisetti, E.L., Roy, S.K., 2000, *Forced convection heat transfer to phase change material slurries in circular ducts*, Journal of thermophysics and heat transfer, 14(1), pp. 115-118.

35. Dinarvand, S., Yousefi, M., Chamkha, A.J., 2022, *Numerical Simulation of Unsteady Flow toward a Stretching/Shrinking Sheet in Porous Medium Filled with a Hybrid Nanofluid*, Journal of Applied and Computational Mechanics, 8(1), pp. 11-20.

36. Kuravi, S., Du, J.,Chow, L.C., 2010, *Encapsulated phase change material slurry flow in manifold microchannels*, Journal of thermophysics and heat transfer, 24(2), pp. 364-373.

37. Buongiorno, J., 2006, *Convective transport in nanofluids*, Journal of heat transfer, 128(3), pp. 240-250.

38. Vand, V., 1945, *Theory of viscosity of concentrated suspensions*, Nature, 155(3934), pp. 364-365.

39. Mulligan, J., Colvin, D., Bryant, Y., 1996, *Microencapsulated phase-change material suspensions for heat transfer in spacecraft thermal systems*, Journal of spacecraft and rockets, 33(2), pp. 278-284.

40. Yamagishi, Y., Takeuchi, H., Pyatenko, A.T., Kayukawa, N., 1999, *Characteristics of microencapsulated PCM slurry as a heat-transfer fluid*, AIChE Journal, 45(4), pp. 696-707.

41. Wang, X., Niu, J., Li, Y., Wang, X., Chen, B., Zeng, R., Song, Q., Zhang, Y., 2007, *Flow and heat transfer behaviors of phase change material slurries in a horizontal circular tube*, International journal of heat and mass transfer, 50(13-14), pp. 2480-2491.

42. Buongiorno, J., Venerus, D.C., Prabhat, N., Mckrell, T., Townsend, J., Christianson, R., Tolmachev, Y.V., Keblinski, P., Hu, L.W., Alvarado, J.L., 2009, *A benchmark study on the thermal conductivity of nanofluids*, Journal of Applied Physics, 106(9), 094312.

43. Venerus, D.C., Buongiorno, J., Christianson, R., Townsend, J., Bang, I.C., Chen, G., Chung, S.J., Chyu, M., Chen, H.,Ding, Y., 2010, *Viscosity measurements on colloidal dispersions (nanofluids) for heat transfer applications*, Applied rheology, 20(4), 44582.

44. Ghalambaz, M., Doostani, A., Izadpanahi, E., Chamkha, A., 2017, *Phase-change heat transfer in a cavity heated from below: the effect of utilizing single or hybrid nanoparticles as additives*, Journal of the Taiwan Institute of Chemical Engineers, 72, pp. 104-115.

45. Shampine, L.F., Kierzenka, J., Reichelt, M.W., 2000, *Solving boundary value problems for ordinary differential equations in MATLAB with bvp4c*, Tutorial notes, pp. 1-27.

46. Bejan, A., 2013, pp. 186-189, *Convection heat transfer*, John Wiley & Sons, New Jersey, United States.

47. Rao, Y., Dammel, F., Stephan, P., Lin, G., 2007, *Convective heat transfer characteristics of microencapsulated phase change material suspensions in minichannels*, Heat and Mass transfer, 44(2), pp. 175-186.

48. Hasan, M.I., 2017, *Improving the cooling performance of electrical distribution transformer using transformer oil–Based MEPCM suspension*, Engineering Science and Technology, an International Journal, 20(2), pp. 502-510.

49. Li, W., Wan, H., Jing, T., Li, Y., Liu, P., He, G., Qin, F., 2019, *Microencapsulated phase change material (MEPCM) saturated in metal foam as an efficient hybrid PCM for passive thermal management: A numerical and experimental study*, Applied Thermal Engineering, 146, pp. 413-421.

50. Siao, Y.H., Yan, W.M., Lai, C.M., 2015, *Transient characteristics of thermal energy storage in an enclosure packed with MEPCM particles*, Applied Thermal Engineering, 88, pp. 47-53.